

Common occurrences of subsurface heatwaves and cold spells in ocean eddies

<https://doi.org/10.1038/s41586-024-08051-2>

Qingyou He^{1,2}, Weikang Zhan^{1,2}, Ming Feng³, Yankun Gong¹, Shuqun Cai^{1,4} & Haigang Zhan^{1,2,4}✉

Received: 28 January 2024

Accepted: 13 September 2024

Published online: 16 October 2024

Open access

 Check for updates

Extreme ocean temperature events are becoming increasingly common due to global warming, causing catastrophic ecological and socioeconomic impacts^{1–5}. Despite extensive research on surface marine heatwaves (MHWs) and marine cold spells (MCSs) based on satellite observations^{6,7}, our knowledge of these extreme events and their drivers in the subsurface ocean—home to the majority of marine organisms—is very limited^{8,9}. Here we present global observational evidence for the important role of mesoscale eddies in the occurrence and intensification of subsurface MHWs and MCSs. We found that 80% of measured MHWs and MCSs below a depth of 100 m do not concur with surface events. In contrast to the weak link between surface MHWs (MCSs) and ocean eddies, nearly one-third of subsurface MHWs (MCSs) in the global ocean, and more than half of such events in subtropical gyres and mid-latitude main current systems, occur within anticyclonic (cyclonic) eddies. These eddy-associated temperature extremes have intensified at rates greater than background level in past decades, suggesting a growing impact of ocean eddies on subsurface MHWs and MCSs with ongoing global warming.

Extreme ocean temperature events, also known as marine heatwaves (MHWs) for prolonged high-temperature extremes and marine cold spells (MCSs) for prolonged low-temperature extremes, exert devastating and, in some cases, irreversible impacts on marine biodiversity, ecosystem functioning and fishery revenues^{1,5,10}. These extreme events are receiving rapidly growing scientific and public attention as the frequency, intensity, duration and spatial extent of MHWs have increased substantially over past decades when using a fixed baseline for their detection, and are projected to be further exacerbated by global warming^{2–4}. The growing threat of ocean temperature extremes highlights the imperative need for a comprehensive understanding of their characteristics and drivers, which is a prerequisite for successfully predicting such events and subsequently implementing proactive marine resource management^{8,11,12}.

The majority of previous studies on MHWs and MCSs have focused on surface signals, largely due to the wide availability of satellite observations of sea-surface temperature^{6,7,13}. However, extreme temperature events below the sea surface are of greater ecological concern because they affect the habitat of most marine primary producers (phytoplankton, 0–200 m) and consumers (fish, 200–1,000 m)^{9,14}. Despite a growing recognition of their importance, our understanding of temperature extremes below the ocean surface is very limited due to the sparsity of continuous subsurface temperature observations^{8,15–17}. Recent model simulations suggest MHWs are frequently hidden below the surface¹⁸, but the results are limited to the upper 200 m and in situ observational validation is needed. More importantly, the physical mechanisms giving rise to these subsurface events remain largely unexplored. Surface MHWs have been demonstrated to be primarily induced by air-sea heat fluxes, current advection and oceanic heat mixing^{15,19,20}, and are

influenced by climate modes such as the El Niño–Southern Oscillation, the Pacific Decadal Oscillation and the Indian Ocean Dipole^{7,12,21,22}. However, the influence of surface thermal forcings on sea-water temperature attenuates with depth and becomes much less pronounced below the well-mixed near-surface layer. This implies that the drivers of subsurface MHWs and MCSs may differ from those of surface events²³.

Oceanic mesoscale eddies, with horizontal scales of the order of 100 km and lifetimes spanning weeks to months, are one of the most ubiquitous and energetic features in the global ocean^{24–26}. These swirling features are widely documented to alter the uptake, redistribution and storage of heat in the ocean^{27–29}. One of the most prominent effects of oceanic eddies is the convergence and downwelling of warm near-surface water in anticyclonic eddies (AEs) and the divergence and upwelling of cold deep water in cyclonic eddies (CEs), resulting in higher temperatures within AEs and lower temperatures within CEs than their surroundings³⁰. In contrast to the attenuation of surface thermal-forcing-induced temperature anomalies with depth, eddy-induced temperature anomalies are more pronounced in the subsurface layer and their effect can extend to depths of over 1,000 m (refs. 25,31). This implies that, in the subsurface ocean, eddies may play a more important role in enhancing local temperature variability and inducing extreme temperature anomalies than at the sea surface³². However, with the exception of a few studies based on long-term, continuous in situ observations at select locations^{23,33}, little is known about the specific impact of mesoscale eddies on subsurface MHWs and MCSs in the global ocean.

In this study, we conducted a global assessment of subsurface MHWs and MCSs through a comprehensive analysis of long-term temperature observations from eight mooring sites in various ocean basins

¹State Key Laboratory of Tropical Oceanography, South China Sea Institute of Oceanology, Chinese Academy of Sciences, Guangzhou, China. ²Guangdong Key Lab of Ocean Remote Sensing, South China Sea Institute of Oceanology, Chinese Academy of Sciences, Guangzhou, China. ³CSIRO Environment, Crawley, Western Australia, Australia. ⁴University of Chinese Academy of Sciences, Beijing, China. ✉e-mail: hgzhhan@sccio.ac.cn

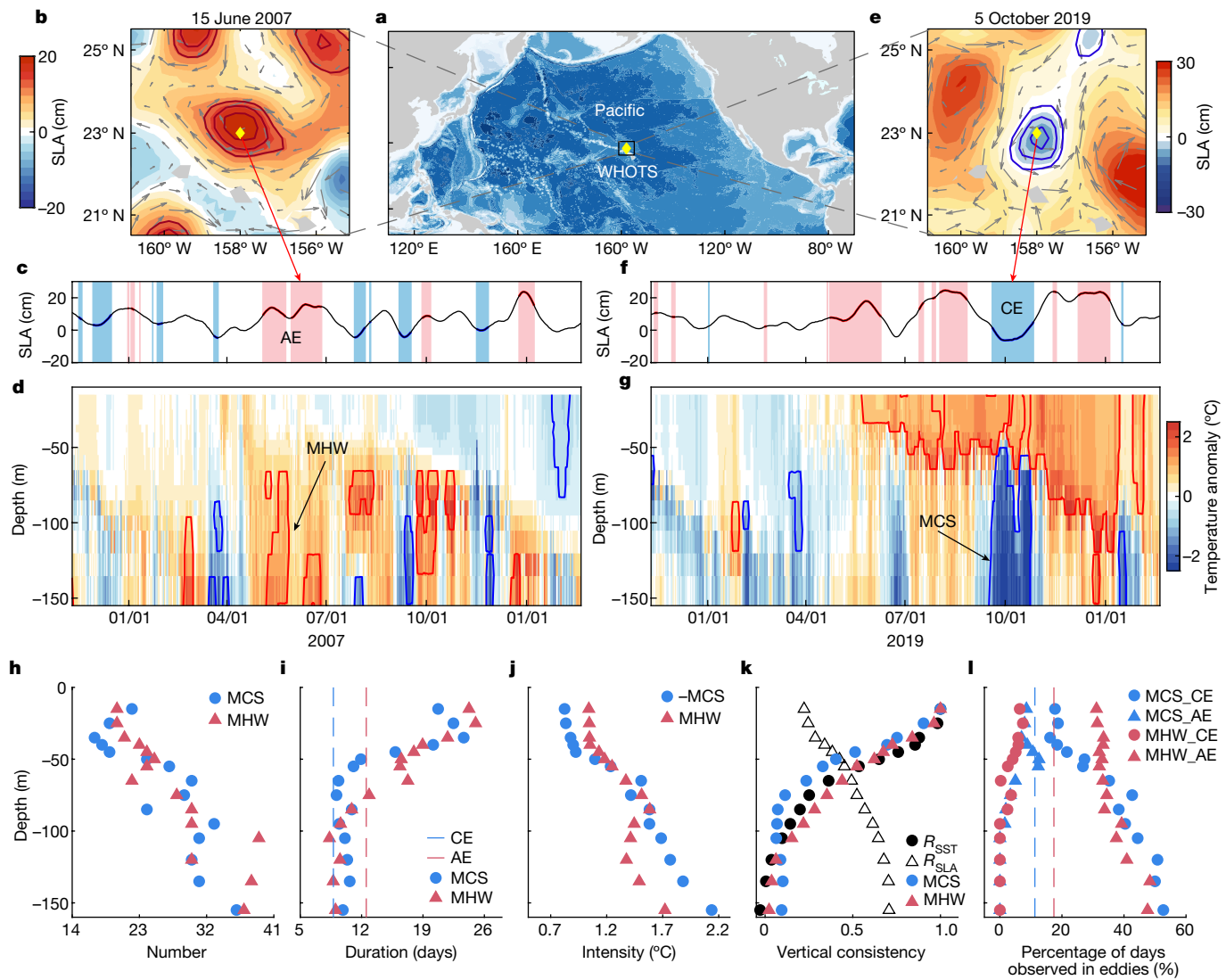


Fig. 1 | Vertical decoupling of subsurface MHWs and MCSs from surface events. **a**, Position of the WHOTS mooring site in the North Pacific Ocean. **b**, Example of an AE passing through the mooring site (yellow) on 15 June 2007. The colours represent SLAs and the vectors are geostrophic velocity anomalies. The shape of the AE is outlined by red contours. **c**, Temporal evolution of SLA at the mooring site in 2007. The passage of AEs and CEs are marked by pink and blue shading, respectively. **d**, Corresponding mooring observations of sea-water temperature anomalies in the upper 155 m. The red and blue lines represent identified MHWs and MCSs, respectively. **e–g**, The same as for **b–d**, but for the passage of a CE in October 2019. **h–j**, Vertical variations in the number (**h**), mean duration (**i**) and mean intensity (**j**) of MHWs (pink triangles) and MCSs (blue dots) identified from each observation depth at the site during

the observation period of August 2004 to March 2020 (Extended Data Fig. 2). **i**, The pink and blue dashed lines are the mean durations of the AEs and CEs passing through the mooring site, respectively. **k**, Vertical consistency of MHWs estimated as a percentage of MHW days at depths with co-occurring surface (15 m) MHW signals (pink triangles). The blue dots represent MCSs. The black dots and triangles are temporal correlation coefficients between temperature anomalies at depth and near the surface (R_{SST}) and those between temperature anomalies at depth and SLAs (R_{SLA}), respectively. **l**, Vertical distributions of the percentages of MHW (pink) and MCS (blue) days observed within AEs (triangles) and CEs (dots), respectively. The pink and blue dashed lines represent the frequency of AE and CE occurrences, respectively.

and over two million global historical temperature-profile measurements (Extended Data Fig. 1 and Extended Data Table 1). Together with co-located satellite-based eddy observations, we reveal the crucial role of eddies in driving and intensifying subsurface MHWs and MCSs in the global ocean.

Mooring site observations

Long-term mooring observations enable a direct estimate of the occurrence of ocean temperature extremes and their vertical structure. For instance, at the Woods Hole Oceanographic Institution Hawaii Ocean Timeseries Site (WHOTS) in the North Pacific Ocean, 20 MHWs (23 MCSs) with a mean duration of 24 (21) days and intensity of 1 (0.8) °C

were observed near the sea surface (15 m) between August 2004 and March 2020 (Fig. 1 and Extended Data Fig. 2). Both the number and intensity of MHWs and MCSs increase with depth, doubling at 155 m, accompanied by a 50% decrease in their duration. In addition, the occurrence of MHWs and MCSs in the subsurface layer decouples in time from surface events. Below a depth of 100 m, over 80% of MHW and MCS days do not coincide with surface signals (Fig. 1k). The same decoupling rate has been observed at the other mooring sites in different ocean basins (Extended Data Fig. 3a,b) and is much greater than those derived from model simulations where mesoscale activities are not well resolved¹⁸. This decoupling of subsurface temperature extremes from surface events is in line with the decrease in temporal correlation between subsurface and surface temperature anomalies with depth

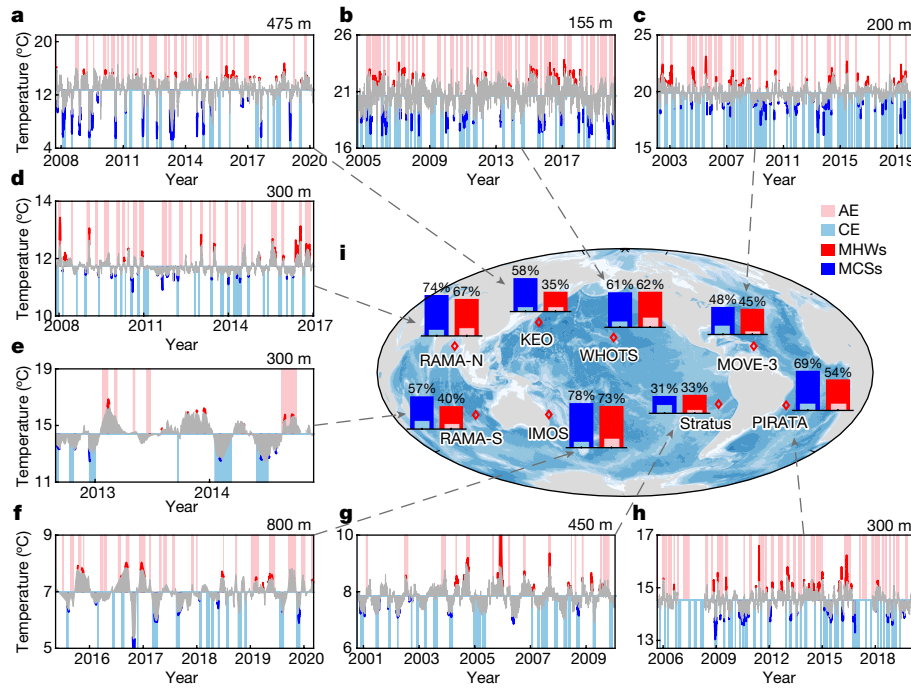


Fig. 2 | Co-occurrence of subsurface MHWs with AEs and MCSs with CEs. **a–h**, Temporal evolution of sea-water temperature (grey) recorded by moorings at various depths in different ocean basins (Extended Data Table 1): KEO (**a**), WHOTS (**b**), MOVE-3 (**c**), RAMA-N (**d**), RAMA-S (**e**), IMOS (**f**), Stratus (**g**) and PIRATA (**h**). The red (blue) patches are MHWs (MCSs). The vertical pink (light blue) shading outlines the periods when the site was inside AEs (CEs). **i**, Corresponding percentages of MHW events co-occurring with AEs (red) and MCSs co-occurring with CEs (blue). The superimposed pink and light blue bars represent the corresponding frequency of eddy occurrence. IMOS, Integrated Marine Observing System; KEO, Kuroshio Extension Observatory; MOVE-3, Meridional Overturning Variability Experiment 3; PIRATA, Prediction and Research Moored Array in the Tropical Atlantic; RAMA-N(S), Research Moored Array for African–Asian–Australian Monsoon Analysis and Prediction–North(South).

(Fig. 1k and Extended Data Fig. 3c). By comparison, the evolution of subsurface temperature is more closely related to that of sea-level anomaly (SLA) (Extended Data Fig. 3d), implying a greater influence of ocean dynamics than air–sea heat exchange on subsurface temperature extremes.

Satellite-based eddy observations show that the WHOTS was located within (one radius of) AEs (CEs) for 17% (11%) of the observation period (Fig. 1b–g,i). However, the mooring observations show that, near the sea surface, 31% (18%) of the MHW (MCS) days were observed within AEs (CEs) (Fig. 1l). This increased occurrence of temperature extremes within eddies seems to support previous model simulations that eddies are important drivers of surface MHWs³⁴. However, the surface events do not coincide closely in time with the occurrence of eddies and also last longer than the duration of the eddies passing through the site (Fig. 1l and Extended Data Fig. 2a). These features suggest that the influence of eddies on surface MHWs and MCSs is likely to be less dominant than other surface forcings¹⁵.

It is interesting that the temporal consistency between temperature extremes and eddies increases with depth (Extended Data Fig. 2). At a depth of 155 m, up to 48% (53%) of the identified MHW (MCS) days were observed within AEs (CEs) (Fig. 1l). By contrast, no MHW (MCS) days were observed within CEs (AEs). When counting the number of extreme events, 20 out of 37 (54%) MHWs co-occurred with AEs, and 18 out of 36 (50%) MCSs co-occurred with CEs (Extended Data Table 2). A similarly high co-occurrence of subsurface MHWs (MCSs) with AEs (CEs) was observed at the other mooring sites (Fig. 2 and Extended Data Fig. 4). This is even more true for extreme MHW (MCS) events above the 95th (below the 5th) percentile of temperature variability (Extended Data Table 2), suggesting an even stronger influence of eddies on more severe extreme temperature events.

The dramatically higher frequency of subsurface MHW (MCS) occurrence within AEs (CEs) than eddy occurrence demonstrates the crucial role of AEs in driving subsurface MHWs and CEs in driving subsurface MCSs. The remaining subsurface MHWs and MCSs occurring outside eddies could be induced by surface heat penetration, wind-forced Ekman transport/pumping, planetary waves and/or convective mixing^{16,17,23,35}. However, most of these features are highly spatiotemporally variable and currently difficult to isolate and track, and are therefore not discussed here.

Global evaluations

Although the mooring observations provide valuable insights into subsurface MHWs and MCSs, they are spatially too sparse to provide a global picture of subsurface temperature extremes. An alternative approach is to make use of millions of historical accumulated temperature-profile data scattered across the global ocean (Extended Data Fig. 1a). Although these profile measurements are spatially and temporally discrete, they are valuable for quantifying regional extreme temperature anomalies³². If these extreme temperature anomalies are temporally continuous MHW/MCS events, they can be used to estimate the influence of eddies on subsurface MHWs (MCSs).

The mooring observations show that, in the upper 1,000 m, approximately 80% of isolated extremely-high-temperature anomaly (EHTA) (extremely-low-temperature anomaly (ELTA)) measurements last for longer than 5 days and qualify as MHWs (MCSs) (Extended Data Fig. 5a,b). In addition, the percentages of EHTA (ELTA) days observed within AEs (CEs) generally equal those of MHW (MCS) days observed within the eddies (Extended Data Fig. 5c,d). To further examine the performance of historical temperature-profile data in measuring temperature extremes, we grouped temperature profiles within $5 \times 5^\circ$ grid boxes centred at each mooring site and compared the estimated extreme temperature statistics with those derived from the mooring observations in the upper 1,000 m (Methods). Recognizing that nearly 20% of extreme temperature anomalies have not been identified as MHWs (MCSs), we increased the criterion for EHTAs (ELTAs) to the 95th (5th) percentile to ensure that most identified extreme temperature anomalies were MHWs (MCSs). The results exhibit high consistency in the extreme statistics between the two datasets for all the mooring sites, except for an underestimation of low-temperature extremes at the Kuroshio Extension Observatory (Fig. 3a,b). An important reason for this underestimation is that the site is positioned on the warm side of the Kuroshio Extension. The equatorward movement of CEs from the north side of the current front carries cold water to this site³⁶, resulting in anomalous low-temperature extremes with magnitudes much greater than the high-temperature extremes (Fig. 2a). However, the profiles in the statistical grid box encompass measurements from both sides of the front, thereby leading to an underestimation of the low-temperature extremes. Overall, although the profile data

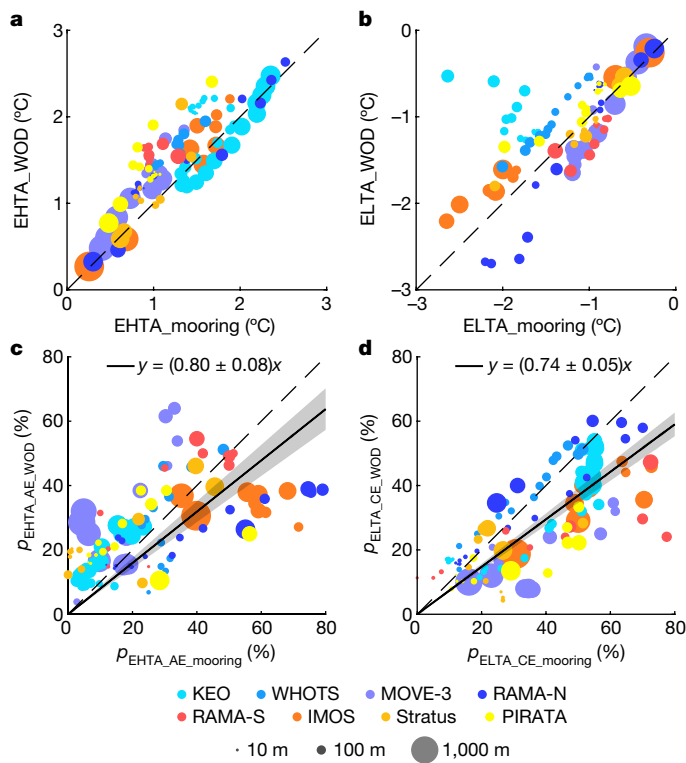


Fig. 3 | Consistency between extreme temperature anomalies estimated from mooring observations and historical temperature-profile measurements. **a**, Scatterplots of 95th percentile EHTAs estimated from the mooring sites and the corresponding historical temperature-profile measurements within $5 \times 5^\circ$ grid boxes centred on the mooring sites. The colours indicate observations from different sites and the size of the dots denotes observation depths from 10 to 1,000 m. **b**, Same as for **a**, but for 5th percentile ELTAs. Note that ELTAs below -3°C (at the KEO site) are not plotted. **c,d**, Same as for **a** (**c**) and **b** (**d**), but for the percentages (*p*) of EHTA measurements observed within AEs (**c**) and ELTA measurements observed within CEs (**d**). The solid black lines with grey shading represent corresponding linear regressions with 95% confidence levels.

underestimate the occurrence of MHWs (MCSs) within AEs (CEs) by approximately 20%, they effectively capture the substantial influence of eddies on subsurface temperature extremes at these sites (Fig. 3c,d).

The effectiveness of the profile dataset in measuring regional extreme temperature anomalies supports a global analysis of temperature extremes below the sea surface. The results show rich geographic variability in the intensity of subsurface extreme temperature anomalies across the global ocean. For example, at 200 m, the magnitudes of EHTAs and ELTAs exceed 2°C in mid-latitude main current systems, such as the Kuroshio Extension, the Gulf Stream, the Brazil Malvinas Confluence and the Antarctic Circumpolar Current (Fig. 4a,b). Similarly high extreme temperature anomalies were observed in these regions throughout the upper 1,000 m (Extended Data Fig. 6), being much stronger than detected in previous model simulations¹⁸. By contrast, those in tropical and subtropical regions are predominantly intense in the upper 500 m, with vertical peak values ranging from 1 to 3°C between 100 and 300 m, generally near the thermocline³⁵.

The percentage of high (low)-temperature extremes observed within AEs (CEs) is, on average, 30% globally at a depth of 200 m, with especially high values exceeding 60% in the mid-latitude main current systems and subtropical gyres (Fig. 4c,d), dramatically higher than the frequency of eddy occurrence (approximately 10%) (Extended Data Fig. 1b,c). In the main current regions, the heightened occurrence of temperature extremes within eddies extends to depths of over 1,000 m (Extended Data Fig. 7), aligning with the energetic and deep-penetrating eddy

signals in these regions^{25,37}. Although eddies in the subtropical gyres are relatively weak, their kinetic energy is nearly an order of magnitude greater than local mean kinetic energy (Extended Data Fig. 1d–f). This dominance of eddy energy over mean currents suggests that eddies may be a primary dynamical process regulating subsurface temperature extremes in the gyre systems. Note that this eddy effect weakens dramatically below a depth of 500 m, possibly due to the inhibition of eddy penetration by the high vertical stratification in these regions³⁸. In tropical oceans, eddies are relatively rare and much less energetic than large-scale currents, resulting in their relatively low contribution to subsurface temperature extremes. Note that, near the surface of the global ocean, generally less than 20% of high (low)-temperature extremes are observed within AEs (CEs) (Extended Data Fig. 7), supporting the mooring observations that the influence of eddies on surface MHWs and MCSs is much weaker than on subsurface events.

The crucial role of eddies in driving subsurface temperature extremes is supported by the decreasing occurrence frequency of extreme temperature anomalies away from the eddy centre. At a global scale, the occurrence frequency of high (low)-temperature extremes is three times higher at the centre of AEs (CEs) compared to eddy peripheries (Fig. 4e). Furthermore, within eddies, both the occurrence frequency and intensity of temperature extremes show a significant rise with an increase in eddy intensity (amplitude) (Fig. 4f,g). For instance, by definition here, the mean occurrence frequency of temperature extremes is 5%. However, within intense AEs (CEs) with amplitudes greater than 20 cm, the occurrence frequency of high (low)-temperature extremes exceeds 25% (Fig. 4f). The probability increases further to one-third for extremely intense eddies with amplitudes greater than 40 cm, which is more than five times greater than the mean occurrence frequency of temperature extremes. A similar phenomenon is observed in subregional statistics in mid-latitude main current systems and subtropical gyres with reasonable regional variability (Extended Data Fig. 8).

Recent trends

The global ocean has experienced significant warming due to increased greenhouse gas emissions in recent decades^{39,40}. To investigate how subsurface MHWs and MCSs have responded to this change, we estimated the linear trends of extreme temperature anomalies in ten different dynamic regions between 1993 and 2019 (Methods). The results show significant positive trends for high-temperature extremes ($0.1\text{--}1^\circ\text{C}$ per decade) in the upper 1,000 m for most regions, except in the Kuroshio Extension (Fig. 5), that are notably greater than the rates of ocean warming⁴¹. The trends remain largely unchanged when the mean-state warming is removed (Extended Data Fig. 9), suggesting that the intensification in the high-temperature extremes is mainly attributable to an enhancement in temperature variability rather than mean-state warming. By comparison, the trends for low-temperature extremes are near zero for most regions and depths, unlike the surface MCSs which tend to have weakening (warming) trends¹⁰. This faster increase in high-temperature extremes than mean-state warming and low-temperature extremes suggests a warming ocean with more pronounced temperature variability.

In addition, we estimated the linear trends in extreme temperature anomalies within eddies. For most of the regions, the trends in high-temperature extremes within AEs are greater and the low-temperature extremes within CEs are lesser than those estimated from all profile measurements (Fig. 5). This suggests a contribution of eddies to magnifying the warming rate of MHWs and the cooling rate of MCSs in the global ocean. On one hand, the warming of the ocean is accompanied by an enhancement in eddy activity^{26,37}, which may produce greater temperature anomalies due to a greater vertical displacement of isothermals^{25,42}. It is evident that eddies with greater intensity exhibit greater temperature extremes compared to weaker ones (Fig. 4g). Additionally, the regions with faster increasing rates in

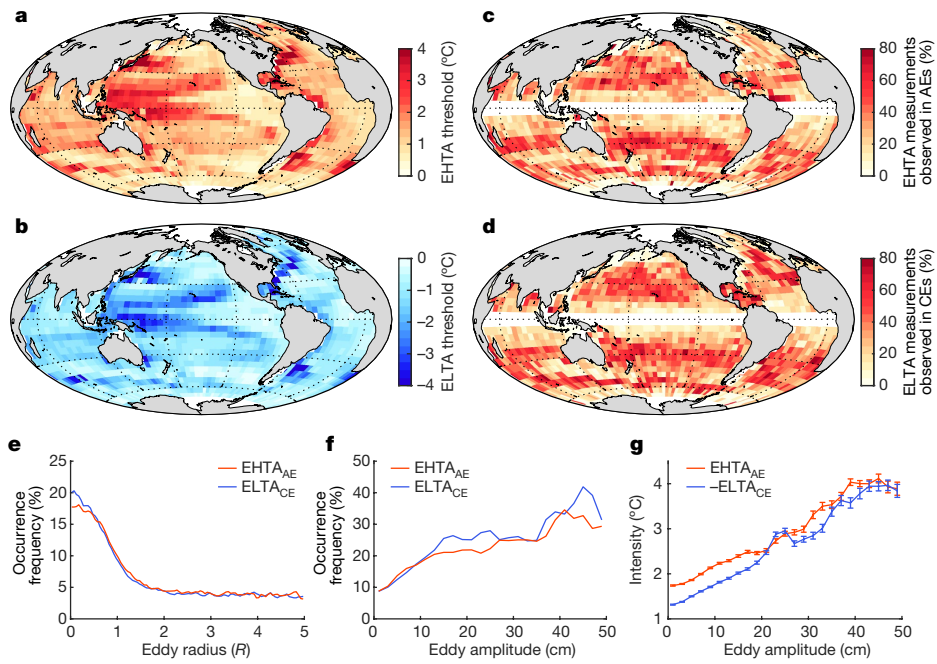


Fig. 4 | Global distributions of the percentages of extreme temperature measurements observed within eddies at 200 m. **a,b**, Thresholds for EHTAs (**a**) and ELTAs (**b**) estimated within each $5 \times 5^\circ$ grid box in the global ocean. **c,d**, Percentages of EHTA measurements observed within AEs (**c**) and ELTA measurements observed within CEs (**d**). Note that the results equatorwards of 5° of latitude are excluded because most mesoscale features at these low latitudes are tropical instability waves²⁴. **e**, Histogram of the occurrence frequency of EHTAs (ELTAs) as a function of normalized distance (by eddy radius) away from the eddy centre. The orange and blue lines represent profiles associated with AEs and CEs, respectively. **f**, Percentages of profiles inside AEs identified as EHTAs (orange) and inside CEs identified as ELTAs (blue) as a function of eddy amplitude. **g**, Same as for **f**, but for the mean intensity of identified EHTAs within AEs (orange) and ELTAs within CEs (blue). The vertical bars represent the corresponding standard errors.

eddy amplitude show faster intensification in temperature extremes within eddies (Fig. 6a). On the other hand, ocean warming weakens with depth⁴¹, accompanied by an increase in vertical stratification in the upper 1,000 m (ref. 38). This increase in vertical temperature gradient may lead to an increase in temperature anomalies forced by the same vertical displacement of isotherms by eddies. This scenario is supported by the greater magnification of extreme temperature trends within eddies in regions with higher stratifying rates (Fig. 6b).

In the ten selected regions, the large-scale vertical temperature gradient in the upper 1,000 m is on the order of 1°C per 100 m. Assuming the subsurface temperature anomalies within eddies are caused solely by the vertical displacement of isotherms, an estimated extreme temperature anomaly of 1°C implies a vertical isothermal displacement of about 100 m. For eddies with a typical surface elevation (amplitude) of 10 cm, the vertical isothermal displacement is around 100 m (refs. 25,43). Over past decades, eddy amplitude in these regions has increased at a rate of $O(1\text{ cm per decade})$, suggesting an amplification of the vertical isothermal displacement of $O(10\text{ m per decade})$ and hence an increase in extreme temperature anomaly of $O(0.1^\circ\text{C per decade})$, which is on the same order of magnitude as the observations (Fig. 6a). By contrast, the increase in the large-scale vertical temperature gradient is on the order of 0.1°C per 1,000 m per decade (Fig. 6b), suggesting an increase in extreme temperature anomaly of 0.01°C per decade for a typical vertical isothermal displacement of 100 m by an eddy. This indicates that the increase in extreme temperature anomaly arising from the increase in vertical stratification is an order of magnitude smaller than that from the increase in eddy intensity. Note that, in mid-latitude main current frontal regions, eddy-associated temperature anomalies are also influenced by large-scale horizontal temperature gradients, for which the trends cannot be estimated from the discrete profile measurements, and their contribution is not assessed here.

Summary and implications

Characterizing extreme temperature events below the ocean surface has long been a challenging task due to the lack of long-term in situ observations. In this study, we analysed the daily evolution of sea-water temperatures recorded by eight mooring sites in various ocean basins, and show that the occurrence of the majority of subsurface MHWs and MCSs do not concur with surface events (Fig. 1

and Extended Data Fig. 3). Our results demonstrate that the observed decoupling of subsurface MHWs and MCSs from surface events is even greater than previously revealed by model simulations¹⁸. These findings also provide a reasonable explanation for previous observations of various vertical temperature structures of surface MHWs^{44,45}. This decoupling suggests that MHWs and MCSs in the subsurface ocean differ fundamentally in their occurrence and possibly physical mechanisms from those at the sea surface, highlighting the importance of the specific observation and investigation of subsurface MHWs and MCSs.

The combination of in situ measurements and satellite eddy observations demonstrates that, although AEs (CEs) occurred in only about 10% of the observation periods, they were responsible for more than half of the subsurface MHWs (MCSs) in subtropical gyres and mid-latitude main current systems (Fig. 4). Although not all eddies can induce subsurface extreme temperature events, the occurrence probability of high (low)-temperature extremes near the centre of AEs (CEs) is much higher than outside eddies (Fig. 4e). For an intense eddy with an amplitude greater than 20 cm, the probability of it being associated with a subsurface extreme temperature event can be up to 25%, surpassing the mean occurrence frequency of temperature extremes by more than four times (Fig. 4f). Given that these results are based on the profile measurements, which may have underestimated the influence of eddies on subsurface temperature extremes by 20%, ocean eddies are likely to be the major source of subsurface MHWs and MCSs in these regions.

As areas that are home to the vast majority of marine organisms, MHWs and MCSs in the subsurface ocean are of particular ecological concern^{9,14}. Furthermore, a large portion of temperature extremes co-occur with extremes of acidification, hypoxia and/or low primary productivity^{19,46}. These compound events are starting to receive particular attention because of their joint harmful impacts on marine organisms and ecosystems in comparison with individual extremes^{13,47}. However, to date, our knowledge of the mechanisms responsible for these events is very limited. In this study, we have demonstrated the important role of eddies in driving subsurface MHWs and MCSs (Fig. 1). Given that eddies redistribute not only heat but also nutrients, oxygen and organisms in the ocean^{48,49}, they might also be important drivers of these biogeochemical extremes and even dual or triple compound events. Additionally, we have revealed a growing impact of ocean eddies on MHWs and MCSs with warming of the global ocean (Fig. 5).

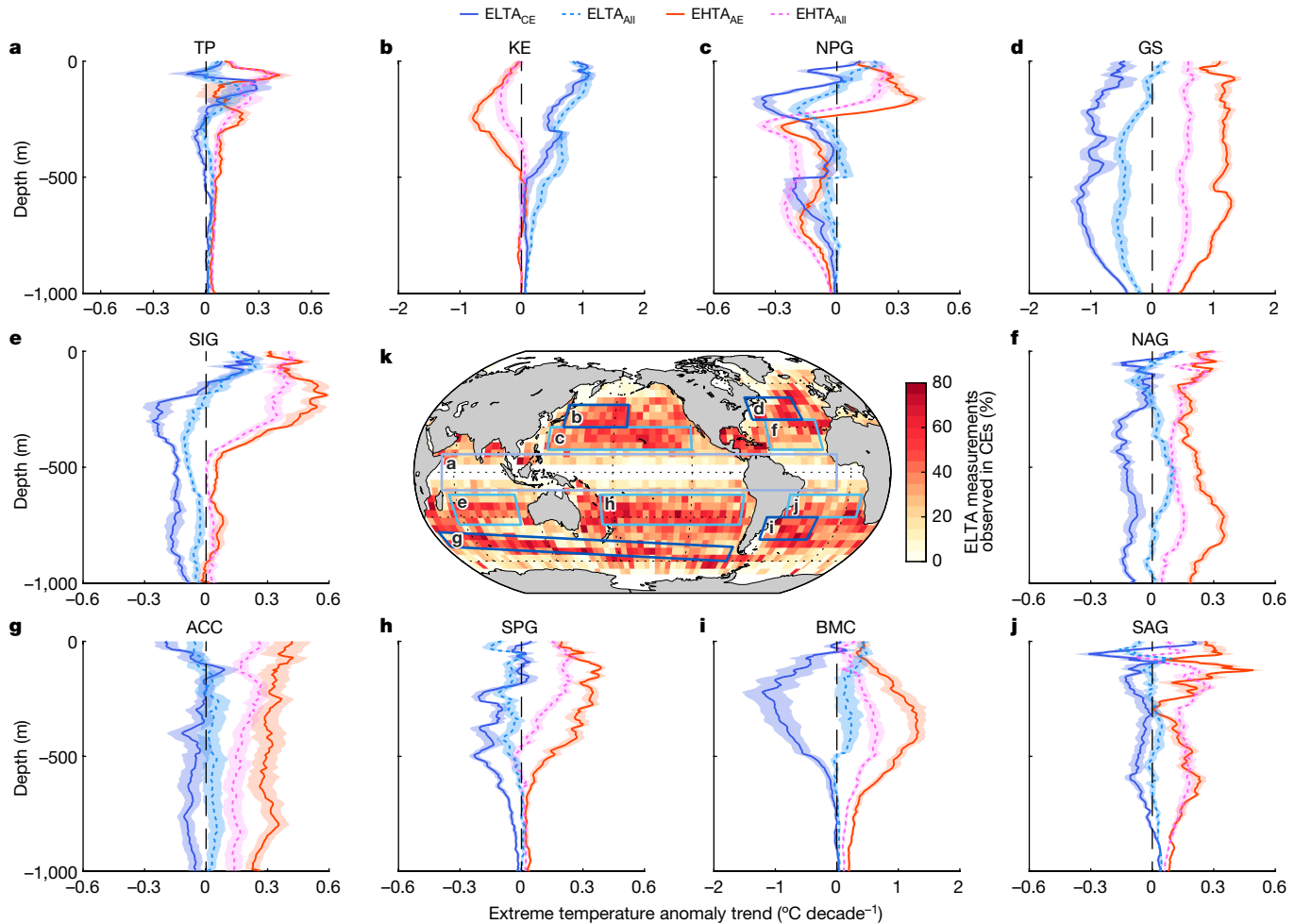


Fig. 5 | Linear trends in regional extreme temperature anomalies between 1993 and 2019. a–j, Linear trends in EHTAs estimated from all historical temperature-profile measurements (EHTA_{All}, magenta) and profiles within AEs (EHTA_{AE}, orange): TP (a), KE (b), NPG (c), GS (d), SIG (e), NAG (f), ACC (g), SPG (h), BMC (i), SAG (j). The dashed blue and solid blue lines represent the linear trends in ELTAs estimated from all profile measurements (ELTA_{All}) and profiles within CEs (ELTA_{CE}), respectively. The shading represents the corresponding standard

deviations. k, The boxes outline the statistical regions, and the colours are the percentages of ELTA measurements observed within CEs, as displayed in Fig. 4d. ACC, Antarctic Circumpolar Current; BMC, Brazil Malvinas Confluence; GS, Gulf Stream; KE, Kuroshio Extension; NAG, North Atlantic gyre; NPG, North Pacific gyre; SAG, South Atlantic gyre; SIG, southern Indian Ocean gyre; SPG, South Pacific gyre; TP, tropical oceans.

These findings may have important implications for understanding and predicting the changes in MHWs (and MCSs) and their ecological consequences under global warming.

The decoupling of subsurface temperature extremes from surface events adds challenges to the identification of subsurface MHWs and MCSs from surface temperature signals. By comparison, the high

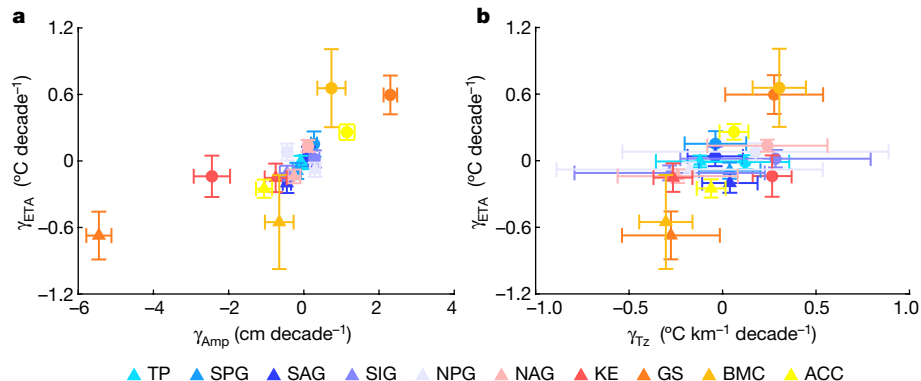


Fig. 6 | Eddy-associated extreme temperature trends as a function of a rise in eddy intensity and vertical stratification. a, Scatterplot of eddy-associated extreme temperature trends (γ_{ETA}) and eddy amplitude trends (γ_{Amp}) in different regions (colours). The circles (triangles) represent mean differences in extremely high (low)-temperature anomaly trends between AEs (CEs) and

regional statistical levels averaged over the upper 1,000 m. The bars represent standard deviations. Note that negative γ_{Amp} for CEs indicates eddy intensification because the SLAs in CEs are negative. b, Same as for a, but for the scatterplot of γ_{ETA} and the trends in regional mean vertical temperature gradients (γ_{Tz}). Note that γ_{Tz} is mirrored negative for CEs.

occurrence of subsurface MHWs within AEs and MCSs within CEs suggests that extreme SLAs may be a practical indicator for subsurface temperature extremes. This hypothesis is supported by the much higher temporal correlation between subsurface temperature anomalies and SLAs than between subsurface and surface temperature anomalies (Extended Data Fig. 3). Given that eddies can now be identified, tracked and even predicted, based on sea-level signals from satellites and model simulations, tracking and predicting potential subsurface MHWs and MCSs using altimeter products may have important applications for disaster warning and management. However, it should be noted that quantifying the intensity of such events requires additional knowledge of the vertical temperature structure. Also, although we have carried out a global estimation of the thresholds of high- and low-temperature extremes within each $5 \times 5^\circ$ grid box in the upper ocean, the profile measurements are unable to determine the horizontal area and temporal evolution of subsurface MHWs (MCSs). Enhanced subsurface observing systems, in combination with satellite observations and eddy-resolved climate models, are needed to further reveal the influence of eddies on the spatial structure and temporal evolution of MHWs (MCSs), as well as their responses to and feedbacks associated with climate change.

Online content

Any methods, additional references, Nature Portfolio reporting summaries, source data, extended data, supplementary information, acknowledgements, peer review information; details of author contributions and competing interests; and statements of data and code availability are available at <https://doi.org/10.1038/s41586-024-08051-2>.

- Smale, D. A. et al. Marine heatwaves threaten global biodiversity and the provision of ecosystem services. *Nat. Clim. Change* **9**, 306–312 (2019).
- Frolicher, T. L., Fischer, E. M. & Gruber, N. Marine heatwaves under global warming. *Nature* **560**, 360–364 (2018).
- Xu, T. et al. An increase in marine heatwaves without significant changes in surface ocean temperature variability. *Nat. Commun.* **13**, 7396 (2022).
- Oliver, E. C. J. et al. Longer and more frequent marine heatwaves over the past century. *Nat. Commun.* **9**, 1324 (2018).
- Welch, H. et al. Impacts of marine heatwaves on top predator distributions are variable but predictable. *Nat. Commun.* **14**, 5188 (2023).
- Jacox, M. G. et al. Global seasonal forecasts of marine heatwaves. *Nature* **604**, 486–490 (2022).
- Holbrook, N. J. et al. A global assessment of marine heatwaves and their drivers. *Nat. Commun.* **10**, 2624 (2019).
- Holbrook, N. J. et al. Keeping pace with marine heatwaves. *Nat. Rev. Earth Environ.* **1**, 482–493 (2020).
- Martin, A. et al. The oceans' twilight zone must be studied now, before it is too late. *Nature* **580**, 26–28 (2020).
- Schlegel, R. W., Darmaraki, S., Benthuysen, J. A., Filbee-Dexter, K. & Oliver, E. C. J. Marine cold-spells. *Prog. Oceanogr.* **198**, 102684 (2021).
- Guo, X. et al. Threat by marine heatwaves to adaptive large marine ecosystems in an eddy-resolving model. *Nat. Clim. Change* **12**, 179–186 (2022).
- Hobday, A. J. et al. With the arrival of El Niño, prepare for stronger marine heatwaves. *Nature* **621**, 38–41 (2023).
- Le Grix, N., Zscheischler, J., Laufkötter, C., Rousseaux, C. S. & Frölicher, T. L. Compound high-temperature and low-chlorophyll extremes in the ocean over the satellite period. *Biogeosciences* **18**, 2119–2137 (2021).
- Corne, M. et al. Deep chlorophyll maxima in the global ocean: occurrences, drivers and characteristics. *Global Biogeochem. Cycles* **35**, e2020GB006759 (2021).
- Oliver, E. C. J. et al. Marine heatwaves. *Ann. Rev. Mar. Sci.* **13**, 313–342 (2021).
- Hu, S. et al. Observed strong subsurface marine heatwaves in the tropical western Pacific Ocean. *Environ. Res. Lett.* **16**, 104024 (2021).
- Scannell, H. A., Johnson, G. C., Thompson, L., Lyman, J. M. & Risser, S. C. Subsurface evolution and persistence of marine heatwaves in the northeast Pacific. *Geophys. Res. Lett.* **47**, e2020GL090548 (2020).
- Sun, D., Li, F., Jing, Z., Hu, S. & Zhang, B. Frequent marine heatwaves hidden below the surface of the global ocean. *Nat. Geosci.* **16**, 1099–1104 (2023).
- Gruber, N., Boyd, P. W., Frolicher, T. L. & Vogt, M. Biogeochemical extremes and compound events in the ocean. *Nature* **600**, 395–407 (2021).
- Bian, C., Jing, Z., Wang, H. & Wu, L. Scale-dependent drivers of marine heatwaves globally. *Geophys. Res. Lett.* **51**, e2023GL107306 (2024).
- Sen Gupta, A. et al. Drivers and impacts of the most extreme marine heatwaves events. *Sci. Rep.* **10**, 19359 (2020).
- Ren, X., Liu, W., Capotondi, A., Amaya, D. J. & Holbrook, N. J. The Pacific Decadal Oscillation modulated marine heatwaves in the northeast Pacific during past decades. *Commun. Earth Environ.* **4**, 218 (2023).
- Schaeffer, A., Sen Gupta, A. & Roughan, M. Seasonal stratification and complex local dynamics control the sub-surface structure of marine heatwaves in eastern Australian coastal waters. *Commun. Earth Environ.* **4**, 304 (2023).
- Chelton, D. B., Schlax, M. G. & Samelson, R. M. Global observations of nonlinear mesoscale eddies. *Prog. Oceanogr.* **91**, 167–216 (2011).
- Frenger, I., Münnich, M., Gruber, N. & Knutti, R. Southern Ocean eddy phenomenology. *J. Geophys. Res. Oceans* **120**, 7413–7449 (2015).
- Beech, N. et al. Long-term evolution of ocean eddy activity in a warming world. *Nat. Clim. Change* **12**, 910–917 (2022).
- Wang, H., Qiu, B., Liu, H. & Zhang, Z. Doubling of surface oceanic meridional heat transport by non-symmetry of mesoscale eddies. *Nat. Commun.* **14**, 5460 (2023).
- He, Q., Zhan, H. & Cai, S. Anticyclonic eddies enhance the winter barrier layer and surface cooling in the Bay of Bengal. *J. Geophys. Res. Oceans* **125**, e2020JC016524 (2020).
- Villas Bôas, A. B., Sato, O. T., Chaigneau, A. & Castelão, G. P. The signature of mesoscale eddies on the air-sea turbulent heat fluxes in the South Atlantic Ocean. *Geophys. Res. Lett.* **42**, 1856–1862 (2015).
- McGillicuddy, D. et al. Influence of mesoscale eddies on new production in the Sargasso Sea. *Nature* **394**, 263–266 (1998).
- Zhang, Z. et al. Observed 3D structure, generation, and dissipation of oceanic mesoscale eddies in the South China Sea. *Sci. Rep.* **6**, 24349 (2016).
- He, Q. et al. Enhancing impacts of mesoscale eddies on Southern Ocean temperature variability and extremes. *Proc. Natl. Acad. Sci. USA* **120**, e2302292120 (2023).
- Wyatt, A. S. J. et al. Hidden heatwaves and severe coral bleaching linked to mesoscale eddies and thermocline dynamics. *Nat. Commun.* **14**, 25 (2023).
- Bian, C. et al. Oceanic mesoscale eddies as crucial drivers of global marine heatwaves. *Nat. Commun.* **14**, 2970 (2023).
- Fragkoupoloul, E. et al. Marine biodiversity exposed to prolonged and intense subsurface heatwaves. *Nat. Clim. Change* **13**, 1114–1121 (2023).
- Nakano, H., Tsujino, H. & Sakamoto, K. Tracer transport in cold-core rings pinched off from the Kuroshio Extension in an eddy-resolving ocean general circulation model. *J. Geophys. Res. Oceans* **118**, 5461–5488 (2013).
- Martinez-Moreno, J. et al. Global changes in oceanic mesoscale currents over the satellite altimetry record. *Nat. Clim. Change* **11**, 397–403 (2021).
- Li, G. et al. Increasing ocean stratification over the past half-century. *Nat. Clim. Change* **10**, 1116–1123 (2020).
- Johnson, G. C. & Lyman, J. M. Warming trends increasingly dominate global ocean. *Nat. Clim. Change* **10**, 757–761 (2020).
- Cheng, L., Abraham, J., Hausfather, Z. & Trenberth, K. E. How fast are the oceans warming? *Science* **363**, 128–129 (2019).
- Roemmich, D. et al. Unabated planetary warming and its ocean structure since 2006. *Nat. Clim. Change* **5**, 240–245 (2015).
- He, Q. et al. Thermal imprints of mesoscale eddies in the global ocean. *J. Phys. Oceanogr.* **54**, 1991–2009 (2024).
- Zhang, Z., Wang, W. & Qiu, B. Oceanic mass transport by mesoscale eddies. *Science* **345**, 322–324 (2014).
- Zhang, Y., Du, Y., Feng, M. & Hobday, A. J. Vertical structures of marine heatwaves. *Nat. Commun.* **14**, 6483 (2023).
- Elzahaby, Y. & Schaeffer, A. Observational insight into the subsurface anomalies of marine heatwaves. *Front. Mar. Sci.* **6**, 745 (2019).
- Le Grix, N., Zscheischler, J., Rodgers, K. B., Yamaguchi, R. & Frölicher, T. L. Hotspots and drivers of compound marine heatwaves and low net primary production extremes. *Biogeosciences* **19**, 5807–5835 (2022).
- Burger, F. A., Terhaar, J. & Frolicher, T. L. Compound marine heatwaves and ocean acidity extremes. *Nat. Commun.* **13**, 4722 (2022).
- Benitez-Nelson, C. R. et al. Mesoscale eddies drive increased silica export in the subtropical Pacific Ocean. *Science* **316**, 1017–1021 (2007).
- Atkins, J., Andrews, O. & Frenger, I. Quantifying the contribution of ocean mesoscale eddies to low oxygen extreme events. *Geophys. Res. Lett.* **49**, e2022GL098672 (2022).

Publisher's note Springer Nature remains neutral with regard to jurisdictional claims in published maps and institutional affiliations.



Open Access This article is licensed under a Creative Commons Attribution-NonCommercial-NoDerivatives 4.0 International License, which permits any non-commercial use, sharing, distribution and reproduction in any medium or format, as long as you give appropriate credit to the original author(s) and the source, provide a link to the Creative Commons licence, and indicate if you modified the licensed material. You do not have permission under this licence to share adapted material derived from this article or parts of it. The images or other third party material in this article are included in the article's Creative Commons licence, unless indicated otherwise in a credit line to the material. If material is not included in the article's Creative Commons licence and your intended use is not permitted by statutory regulation or exceeds the permitted use, you will need to obtain permission directly from the copyright holder. To view a copy of this licence, visit <http://creativecommons.org/licenses/by-nc-nd/4.0/>.

© The Author(s) 2024

Article

Methods

Mooring observations

Ocean moorings provide long-term measurements of sea-water temperature, offering a valuable means of investigating subsurface MHWs and MCSs. Currently, most mooring stations are built in tropical oceans¹⁶. Given the typically weak eddy activity in tropical oceans²⁴, most of the mooring data from low latitudes were not analysed in this study. We isolated data from the northernmost (southernmost) site of the Research Moored Array for African–Asian–Australian Monsoon Analysis and Prediction in the northern (southern) Indian Ocean, the southernmost site of the Prediction and Research Moored Array in the Tropical Atlantic in the South Atlantic Ocean, and five additional sites covering diverse dynamical regions across different extratropical ocean basins globally (Extended Data Fig. 1 and Extended Data Table 1). The selection of these sites was a compromise between the availability of mooring data and the representativeness of a broad global ocean region. For each site, observation depths with data coverage shorter than three-quarters of the whole duration of the mooring observation were not considered. Temperature measurements at each observation depth were daily averaged to facilitate the identification of MHWs and MCSs. Data gaps shorter than one month were filled by linear interpolation and those longer than one month were filled with climatological daily mean values estimated from the corresponding mooring.

Historical temperature-profile data

Global temperature-profile data were obtained from the World Ocean Database (WOD), which is a collection of the available historical in situ hydrographic measurements from various platforms, such as ship-based conductivity–temperature–depth, expendable bathythermograph, moored buoy, Argo float and glider, from across the global ocean⁵⁰. In this study, we isolated temperature profiles with quality control flags marked as ‘O’ (accepted) between January 1993 and March 2020. In addition to the initial quality control conducted on the WOD, profiles without temperature observations shallower than 20 m or deeper than 100 m, with less than 10 unique observations in the upper 200 m, and with vertical sampling intervals greater than 15 m between 0 and 100 m and greater than 25 m between 100 and 200 m were discarded²⁸. This process aimed to reduce uncertainties in the vertical linear interpolation of the profile measurements into the standard high-resolution grids, which ranged from 10 to 1,000 m with a depth interval of 5 m. After this filtering, more than two million profiles remained, with most $5 \times 5^\circ$ grid boxes containing more than 1,000 profile measurements (Extended Data Fig. 1a).

Satellite eddy products

Mesoscale eddies are identified and tracked from multi-satellite altimeter data based on overlapping closed contours of sea-surface height (SSH) fields⁵¹. The eddy product (META3.1exp, DT allsat) is available from the Archiving, Validation and Interpretation of Satellite Oceanographic (AVISO) database. This dataset contains daily time series of the position, amplitude, radius, polarity, rotational speed and associated edge contours of each identified and tracked eddy from January 1993 to March 2020. Eddies that rotate clockwise in the Northern Hemisphere and counterclockwise in the Southern Hemisphere are called AEs, while those that rotate in the opposite direction are called CEs. The eddy radius is estimated as the radius of the best fit circle corresponding to the contour of maximum circum-average speed (defined as the eddy edge)⁵¹. The eddy amplitude is defined as the absolute SSH difference between the extremum of SSH within the eddy and the SSH around the effective contour that defines the eddy’s edge. In this study, we estimated the occurrence frequency of AEs (CEs) as the percentage of days when a target point (mooring site) was located in any AEs (CEs) during the sampling period. The SLA and geostrophic velocity anomaly

data used to outline the horizontal structure of the eddies in Fig. 1 was obtained from the Copernicus Marine Environment Monitoring Service.

Identification of MHWs and MCSs

The MHWs and MCSs are identified separately for each observation depth at each mooring site. An MHW is identified as an anomalously warm event with consecutive high water temperatures exceeding a day-of-the-year climatology of the 90th percentile for at least 5 days⁵². Similarly, an MCS is identified as an anomalously cold event with consecutive low water temperatures falling below a day-of-the-year climatology of the 10th percentile for at least 5 days. The climatology values were computed using the whole duration of the corresponding mooring dataset and then smoothed using a 31-day window⁵³. Severe MHWs and MCSs were identified using the thresholds of the 95th and 5th percentile temperatures, respectively. We noted that these mooring sites were built in different years and that the obtained data ranged from 2 to over 20 years. All the mooring observations showed a dramatically higher occurrence of subsurface MHWs (MCSs) within AEs (CEs) than within CEs (AEs), indicating that the length of the mooring data did not influence the findings of this study.

Eddy-associated temperature extremes

For each mooring site, the variation in water temperature is assumed to be influenced by the nearest eddy. Thus, we associated the site with the eddy nearest to it on each sampling day. The distance of the site to the associated eddy was normalized by the radius of the eddy (R) to facilitate the comparison of eddies of different sizes (Fig. 1g,h). Then, the percentage of MHW (MCS) days observed within the interiors (one radius) of AEs and CEs were computed for each observation depth, respectively. For an MHW (MCS) event, if an eddy was detected during the period (any of the MHW (MCS) days was detected within the radius of an eddy), it was defined as co-occurring with the eddy.

To evaluate the performance the WOD temperature profiles in measuring regional temperature extremes, we assumed that the regional variability in extreme temperature statistics in a relatively small region ($5 \times 5^\circ$ grid box) was negligible. We grouped temperature profiles within $5 \times 5^\circ$ grid boxes centred on each of the mooring sites and checked the consistency of the estimated extreme temperature anomalies between the two datasets. Given that nearly 20% of EHTAs (ELTAs) are not identified as MHWs (MCSs) (Extended Data Fig. 5), we increased the criterion for EHTAs (ELTAs) to the 95th (5th) percentile temperature to further ensure that most isolated extreme temperature anomalies were MHWs (MCSs). Before estimating extreme temperature anomalies, each profile measurement was subtracted from the corresponding climatological monthly mean value at the closest matching point, using the World Ocean Atlas 2018 products, to remove seasonal cycle signals and mitigate aliasing due to sparse historical sampling⁵⁴.

Similarly to the association of mooring observations with eddies, we associated each WOD temperature profile with the nearest eddy and normalized the distance between them using the eddy radius²⁸. The influence of eddies on extreme temperature anomalies was clarified by estimating the percentage of EHTA measurements occurring within AEs and the percentage of ELTA measurements occurring within CEs. The horizontal range of the eddies’ influence was specified by estimating the occurrence frequency of EHTAs (ELTAs) as a function of normalized distance away from the centre of AEs (CEs) (Fig. 4e). The sensitivity of extreme temperature anomalies to eddy properties was estimated by analysing the occurrence frequency (and mean intensity) of EHTA (ELTA) measurements inside eddies as a function of eddy amplitude (Fig. 4f,g)⁵⁵.

Linear trends in temperature extremes

Recent trends in temperature extremes were assessed through linear least-squares regression for monthly series of EHTAs and ELTAs

in various dynamical regions. The analysed dynamical regions encompassed tropical oceans (50° E– 350° E, 12° S– 5° S and 5° N– 12° N), subtropical gyres (including the North Pacific gyre (130° E– 240° E and 15° N– 30° N), North Atlantic gyre (300° E– 340° E and 15° N– 35° N), southern Indian Ocean gyre (55° E– 105° E and 35° S– 15° S), South Pacific gyre (170° E– 280° E and 35° S– 15° S) and South Atlantic gyre (315° E– 370° E and 30° S– 15° S)) and mid-latitude main current systems (including the Kuroshio Extension (140° E– 190° E and 33° N– 43° N), Gulf Stream (290° E– 330° E and 35° N– 50° N), Brazil Malvinas Confluence (300° E– 340° E and 45° S– 30° S) and Antarctic Circumpolar Current (shifting polewards linearly from 50° S– 40° S at 35° E to 60° S– 50° S at 280° E) (boxes in Fig. 5k). In each statistical region, the 95th and 5th percentile temperature anomalies were calculated at each depth for each month. Unlike trend estimation based on a fixed threshold for EHTA (ELTA), this approach avoids situations where temperature extremes are exclusively detected in some years (for example, the extremes in Extended Data Fig. 2a). To mitigate the uncertainty stemming from the imbalance of the number of available profiles across different months and years, we employed the random resampling of 100 profiles with replacements in a five-month window centred on each month and then estimated the linear trends of the derived time series. This process was repeated 1,000 times, and the mean value and standard deviation of the derived trends were estimated. The statistical significance of the mean trend was detected using a *t*-test with a *P* value of 0.05.

Data availability

The mooring data was obtained from the OceanSITES website at <https://dods.ndbc.noaa.gov/oceansites/>. The global historical in situ temperature-profile data was derived from the WOD at https://www.ndc.noaa.gov/OC5/WOD/pr_wod.html. The eddy product was provided by the AVISO⁺ website at <https://aviso.altimetry.fr>. The climatology sea-water temperature data (World Ocean Atlas 2018) is available at <https://www.ncei.noaa.gov/access/world-ocean-atlas-2018/>. The SLA and geostrophic velocity anomaly data are publicly available from the Copernicus Marine Environment Monitoring Service at <https://marine.copernicus.eu/>. All analyses were performed using MATLAB, and the base maps for the figures were from M-Map at <https://www.eoas.ubc.ca/~rich/map.html>.

Code availability

The MHW detection at each mooring site and each observation depth used in this study is available at https://github.com/ZijieZhaoMMHW/m_mhw1.0 (ref. 56). Codes for the main results are available via Zenodo at <https://doi.org/10.5281/zenodo.13235274> (ref. 57).

50. Boyer, T. P. et al. *NCEI standard product: World Ocean Database (WOD)* (NOAA National Centers for Environmental Information dataset, accessed 21 October 2021); www.ncei.noaa.gov/access/metadata/landing-page/bin/iso?id=gov.noaa.nodc:NCEI-WOD
51. Pegliasco, C. et al. META3.1exp: a new global mesoscale eddy trajectory atlas derived from altimetry. *Earth Syst. Sci. Data* **14**, 1087–1107 (2022).
52. Hobday, A. J. et al. A hierarchical approach to defining marine heatwaves. *Prog. Oceanogr.* **141**, 227–238 (2016).
53. Gupta, H., Sil, S., Gangopadhyay, A. & Gawarkiewicz, G. Observed surface and subsurface marine heat waves in the Bay of Bengal from in-situ and high-resolution satellite data. *Clim. Dyn.* **62**, 203–221 (2023).
54. Swart, N. C., Gille, S. T., Fyfe, J. C. & Gillett, N. P. Recent Southern Ocean warming and freshening driven by greenhouse gas emissions and ozone depletion. *Nat. Geosci.* **11**, 836–841 (2018).
55. He, Q. et al. A new assessment of mesoscale eddies in the South China Sea: surface features, three-dimensional structures and thermohaline transports. *J. Geophys. Res. Oceans* **123**, 4906–4929 (2018).
56. Zhao, Z. & Marin, M. A MATLAB toolbox to detect and analyze marine heatwaves. *J. Open Source Softw.* **4**, 1124 (2019).
57. He, Q. Codes and source data for “Common occurrences of subsurface heatwaves and cold-spells in ocean eddies”. Zenodo <https://doi.org/10.5281/zenodo.13235274> (2024).

Acknowledgements This work was supported by the National Natural Science Foundation of China (42276027), the Strategic Priority Research Program of the Chinese Academy of Sciences (XDA0370101), the National Natural Science Foundation of China (42130404, 42276186 and 42106169), the Youth Innovation Promotion Association CAS (2021343), the National Science Foundation of Guangdong (2023A1515010966), the National Key R&D Program of China (2023YFC3108002) and the development fund of the South China Sea Institute of Oceanology of the Chinese Academy of Sciences (SCSIO202204 and SCSIO20230Y02).

Author contributions Q.H. and H.Z. conceived the study. Q.H. conducted the analysis and wrote the paper. W.Z., M.F., Y.G., S.C. and H.Z. contributed to the interpretation of the results and the revision of the manuscript.

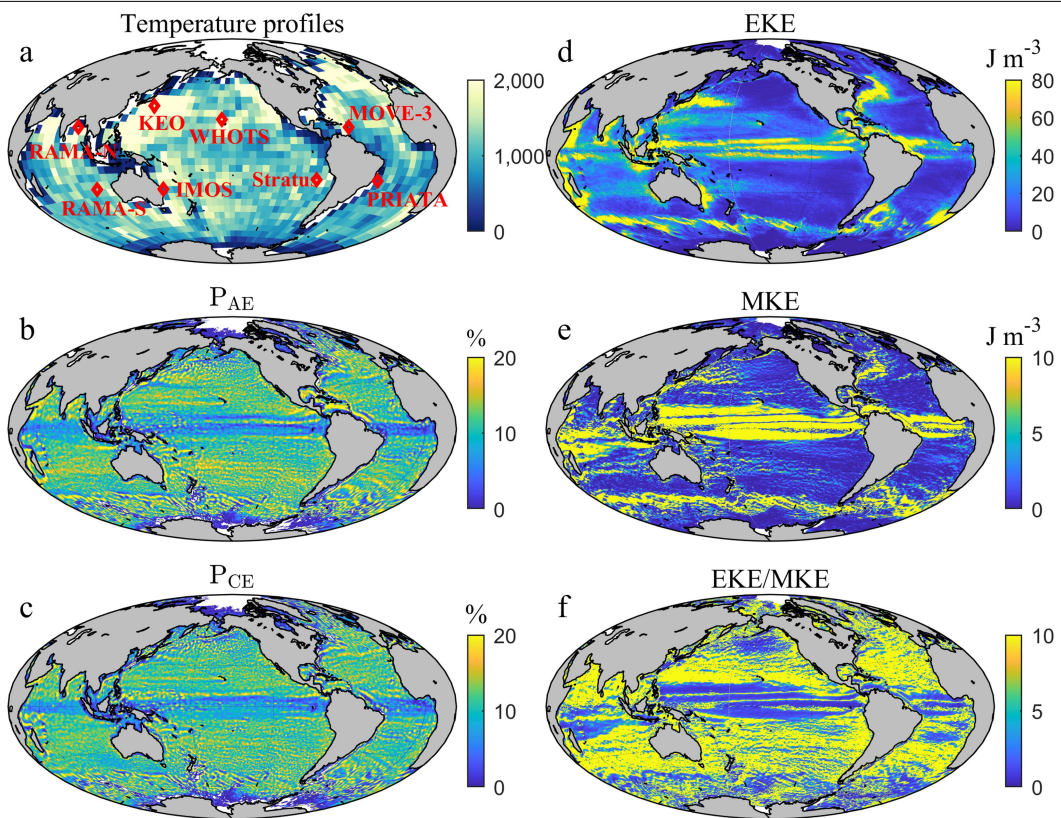
Competing interests The authors declare no competing interests.

Additional information

Correspondence and requests for materials should be addressed to Haigang Zhan.

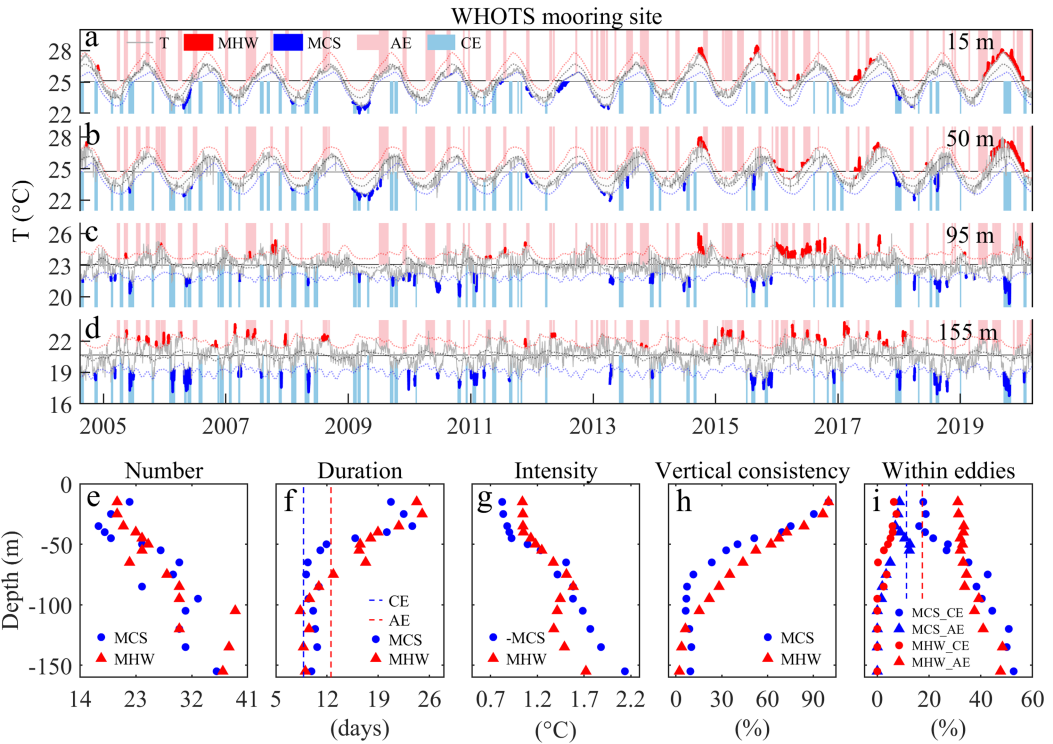
Peer review information *Nature* thanks the anonymous reviewers for their contribution to the peer review of this work.

Reprints and permissions information is available at <http://www.nature.com/reprints>.



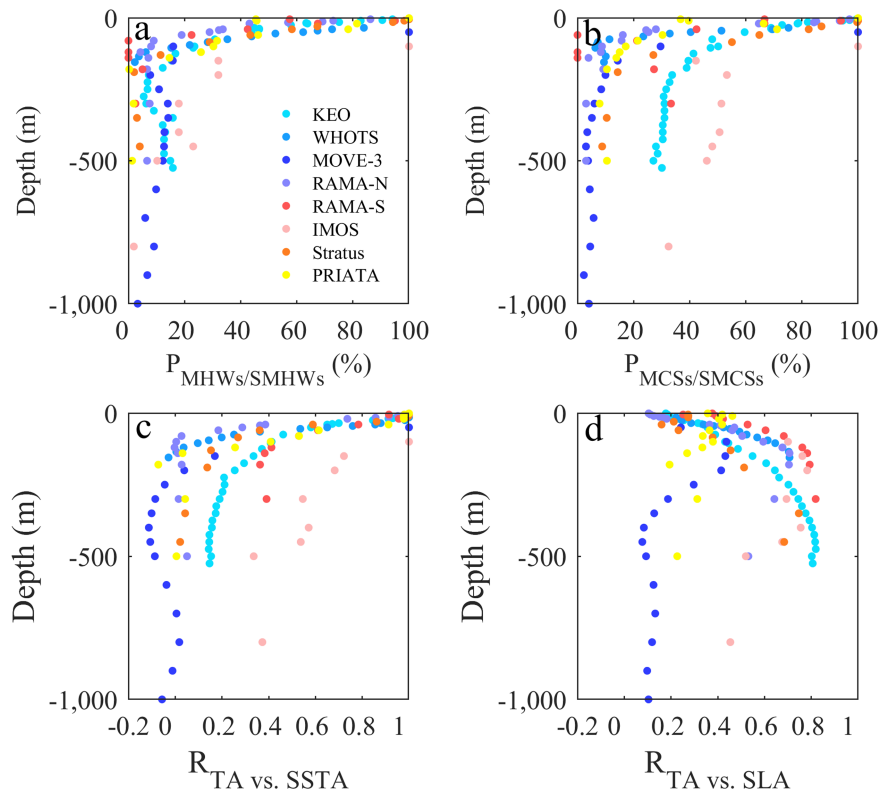
Extended Data Fig. 1 | Global distribution of in situ temperature measurements and satellite eddy data. **a**, Global distribution of historical temperature profile measurements between January 1993 and March 2020. The red diamonds indicate the positions of the mooring sites in Extended Data Table 1. **b,c**, Global distribution of the occurrence frequency of AEs (P_{AE}) and CEs (P_{CE}). **d–f**, Global distribution of time-mean eddy kinetic energy

$EKE = \frac{1}{2}\rho_0(u'^2 + v'^2)$, mean kinetic energy $MKE = \frac{1}{2}\rho_0(\bar{u}^2 + \bar{v}^2)$, and the ratio between them (EKE/MKE) estimated from satellite observations of geostrophic current velocity (u, v). (\bar{u}, \bar{v}) are the time-mean values of (u, v) and $(u' = u - \bar{u}, v' = v - \bar{v})$ are the time-varying components. $\rho_0 = 1025 \text{ kg m}^{-3}$ is the density of seawater³⁷.



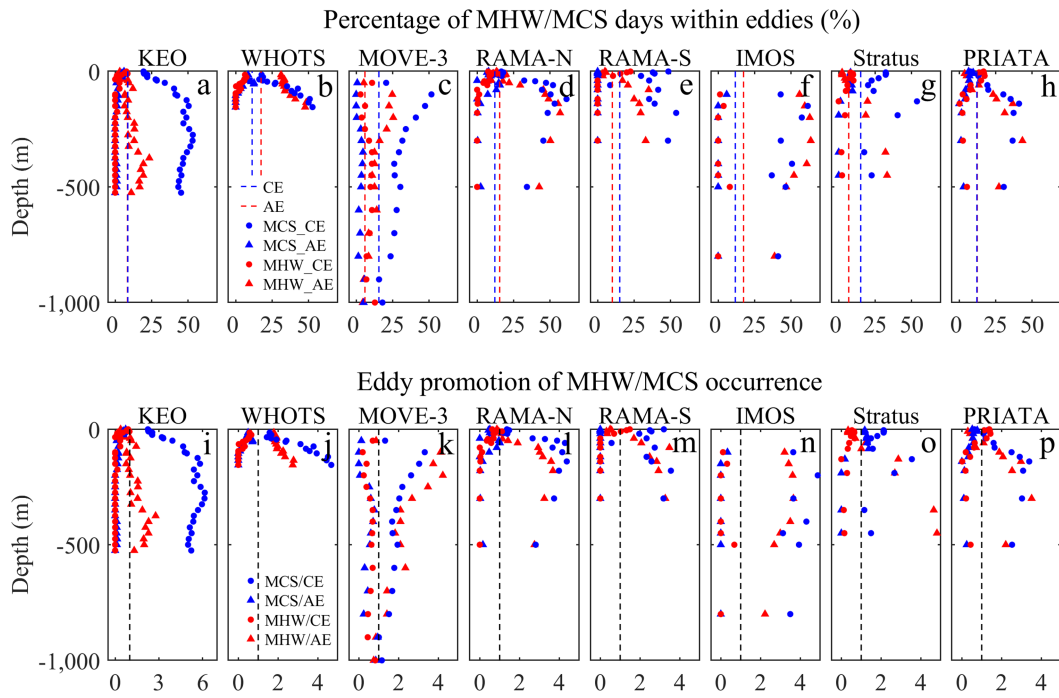
Extended Data Fig. 2 | Vertical variation of MHWs and MCSs at the WHOTS mooring site. **a**, MHWs (red patches) and MCSs (blue patches) identified from daily temperature observations (grey) at depths of 15 m at the WHOTS mooring site. The thin blue, black and red dashed lines are climatological monthly 10th percentile, mean, and 90th percentile temperatures, respectively, estimated from the mooring data between August 2004 and March 2020. The vertical pink (cyan) shadings indicate the periods when the mooring site is inside AEs (CEs), which are identified from satellite altimeter products. **b–d**, The same as **a**, but for the depths of 50 m, 95 m, and 155 m, respectively. **e–g**, Vertical variations of the number, mean duration, and mean intensity of MHWs (red triangles) and MCSs (blue dots) identified from each observation depth of the site during the observation period between August 2004 and March 2020

(Extended Data Fig. 2). The red and blue dashed lines in **i** are the mean durations of AEs and CEs passing through the mooring site, respectively. **h**, Vertical consistency of MHWs estimated as the percentage of MHW days at depths with co-occurring surface (15 m) MHW signals (red triangles). The blue dots are for MCSs. The black dots and triangles are temporal correlation coefficients between temperature anomalies at depths and near the surface (R_{SST}) and those between temperature anomalies at depths and sea level anomaly (R_{SLA}), respectively. **i**, Vertical distributions of the percentages of MHW (red) and MCS (blue) days observed within AEs (triangles) and CEs (dots), respectively. The red and blue dashed lines are the frequency of AE and CE occurrence, respectively. Note that **e–i** are the same as Fig. 1h–l in the main text.



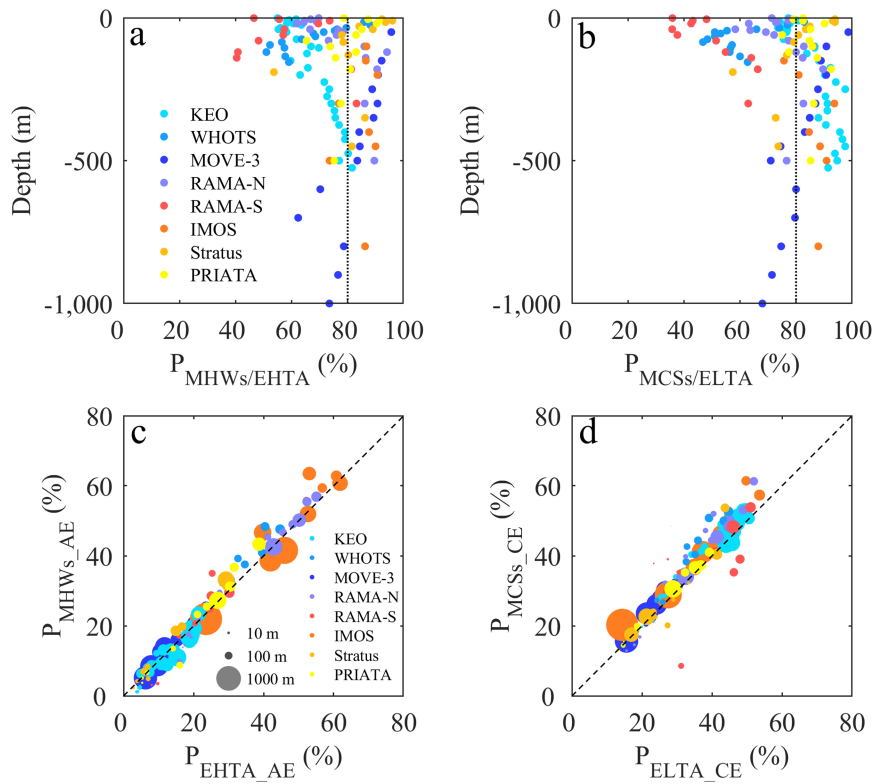
Extended Data Fig. 3 | Consistency between MHWs/MCSs at depths and surface events as a function of depth. **a**, Scatterplots of the percentages of MHW days at depths with co-occurring near-surface MHWs at the shallowest observation depths of the mooring sites. Note that the shallowest depth of temperature measurements at the IMOS site is 100 m (Extended Data Table 1).

b, The same as **a** but for MCSs. **c**, Temporal correlation coefficients between temperature anomalies at depths (TA) and near the surface (SSTA) at the mooring sites. The temperature anomalies are estimated by removing seasonal cycles from the mooring observations. **d**, The same as **c** but for correlation coefficients between TA and sea level anomaly (SLA).



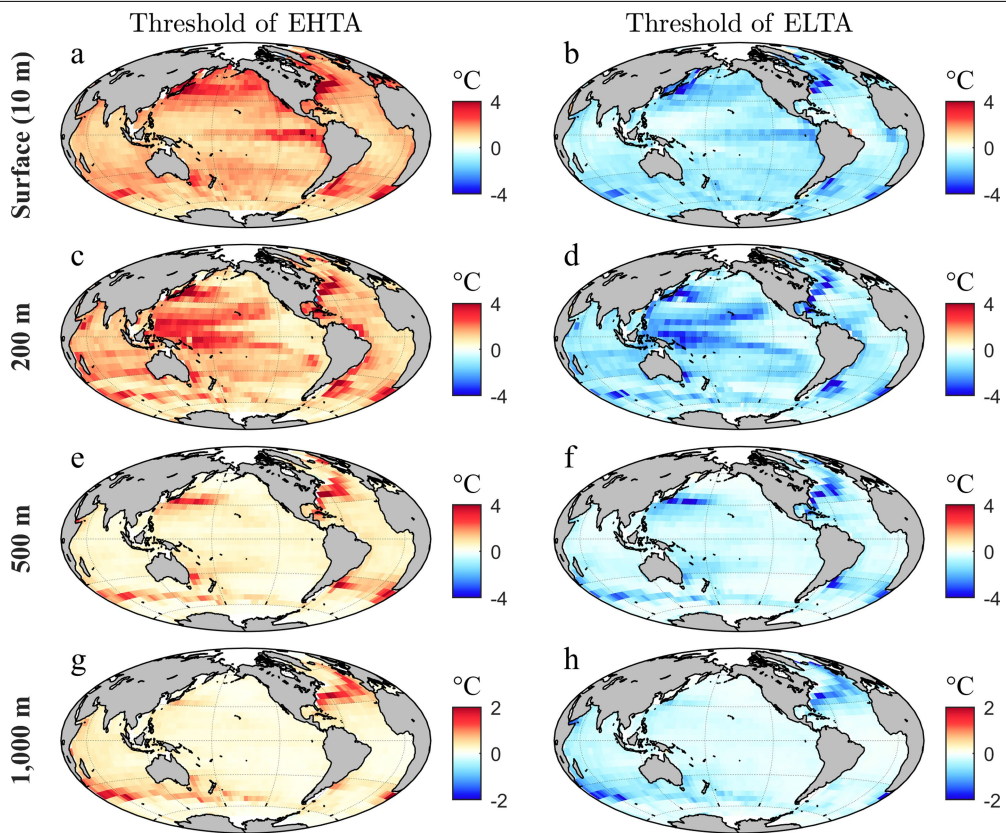
Extended Data Fig. 4 | Influence of eddies on MHWs/MCSs as a function of depth. **a–h**, Vertical distributions of the percentages of MHW days observed within AEs (red triangles) and CEs (red dots) at the observation depths of the 8 mooring sites. The blue colours are for MCS days observed within AEs (blue

triangles) and CEs (blue dots). The red and blue dashed lines are the occurrence frequency of AEs and CEs, respectively. **i–p**, The same as **a–h** but for the ratios between the percentages of MHW (MCS) days observed within eddies and the corresponding occurrence frequency of eddies.



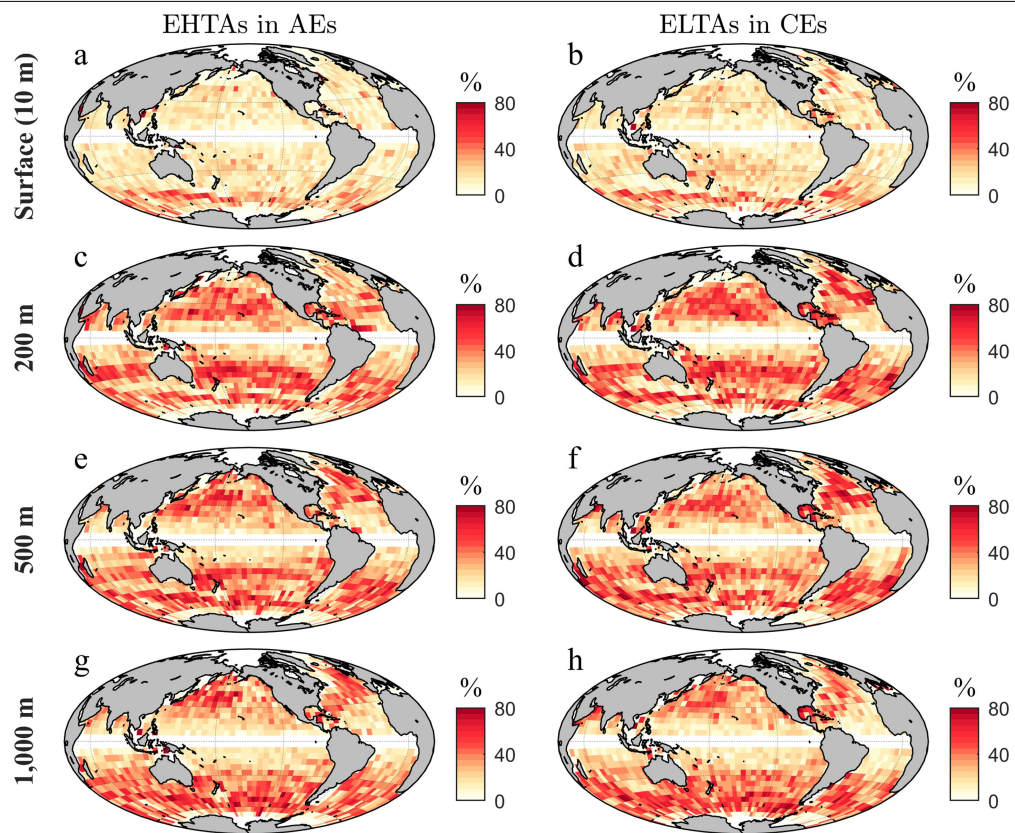
Extended Data Fig. 5 | Percentages of isolated extremely high (low)-temperature anomaly measurements qualify as temporal continuous MHWs (MCSs). **a.**, Scatterplots of the percentages of extremely high-temperature anomaly (EHTA) measurements lasting for longer than 5 days and identified as MHWs at different observation depths of the mooring sites.

b., The same as **a** but for the percentages of extremely low-temperature anomaly (ELTA) measurements identified as MCSs. **c.**, Consistency between the percentages of EHTA days and MHW days observed within AEs. **d.**, The same as **c**, but for ELTA and MCS measurements.



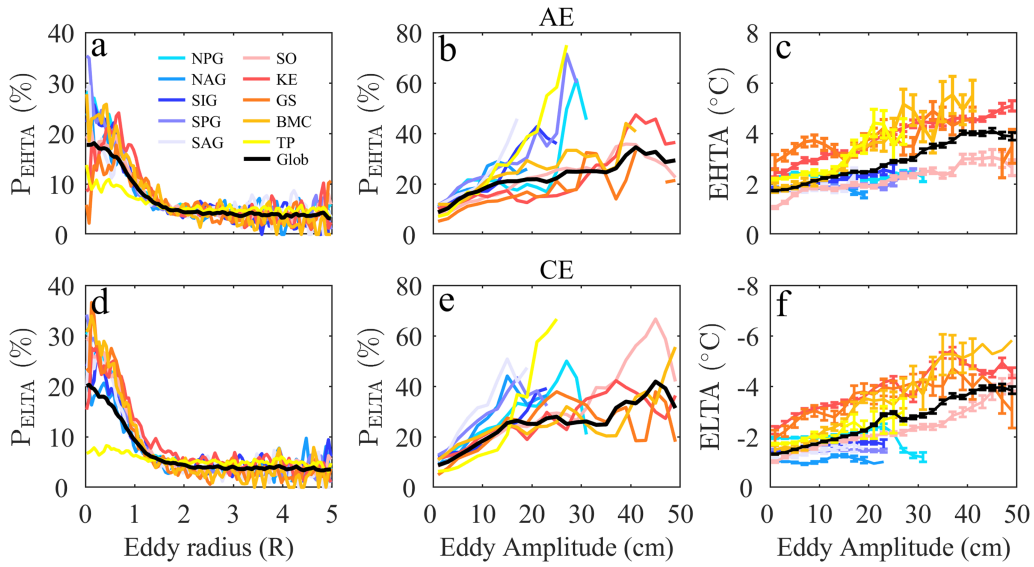
Extended Data Fig. 6 | Horizontal and vertical variability of temperature extremes in the global ocean. **a–h,** Geographic distribution of the thresholds of extremely high-temperature anomaly (left) and extremely low-temperature

anomaly (right) at the depths of (from top to bottom) 10 m, 200 m, 500 m, and 1,000 m, respectively. Panels **c,d** are the same as Fig. 4a,b in the main text.



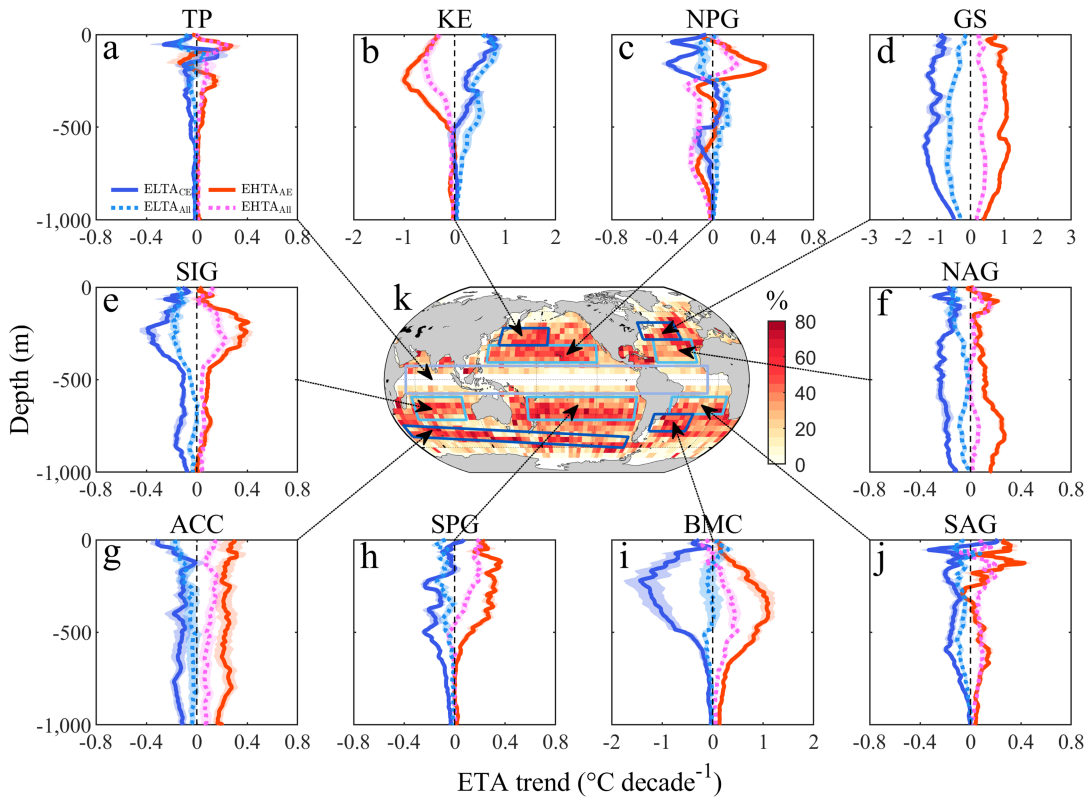
Extended Data Fig. 7 | Horizontal and vertical variability of the influence of eddies on temperature extremes in the global ocean. a–h, Geographic distribution of the percentages of extremely high-temperature anomaly measurements observed within AEs (left) and extremely low-temperature

anomaly measurements observed within CEs (right) at the depths of (from top to bottom) 10 m, 200 m, 500 m, and 1,000 m, respectively. Panels c,d are the same as Fig. 4c,d in the main text.



Extended Data Fig. 8 | The influence of eddy intensity on temperature extremes at the depth of 200 m. **a**, Histogram of the percentage of profile measurements identified as extremely high-temperature anomalies (occurrence frequency of EHTA) as a function of normalized distance (by eddy radius) away from the centre of the nearest eddy in different regions of the global ocean (boxes in Fig. 5k). The black line is for global ocean as in Fig. 4e.

Note that only the profiles associated with AEs are counted here. **b**, The same as **a**, but for the occurrence frequency of EHTAs within AEs as a function of eddy amplitude. **c**, The same as **b**, but for the mean intensity of EHTAs within AEs. The vertical bars are corresponding standard errors. **d–f**, The same as **a–c**, but for extremely low-temperature anomalies (ELTAs) associated with CEs.



Extended Data Fig. 9 | Linear trends of regional extreme temperature anomalies estimated from detrended data. **a–j.** The linear trends of extremely high-temperature anomalies estimated from all historical temperature profile measurements (EHTA_{All}, magenta) and profiles within AEs (EHTA_{AE}, red). Regional mean-state warming trend is removed before the trend analysis. The cyan and blue lines are for the linear trends of extremely

low-temperature anomalies estimated from all profile measurements (ELTA_{All}) and profiles within CEs (ELTA_{CE}), respectively. The shadings are the corresponding standard deviations. The boxes in **k** outline the statistical regions and the colours are the percentages of ELTA measurements observed within CEs as displayed in Fig. 4d.

Extended Data Table 1 | Data from the mooring sites analysed in this study

Site	Latitude (°N)	Longitude (°E)	Observation period	Water depth (m)	Depths of temperature observation (m)
WHOTS	23	202	2004.08-present	4700	15, 25, 35, 40, 45, 50, 55, 65, 75, 85, 95, 105, 120, 135, 155
KEO	32	144	2007.09-present	5700	1, 5, 8, 10, 15, 18, 20, 25, 35, 38, 40, 50, 75, 100, 105, 400, 425, 450, 475, 500, 525
MOVE-3	16	299	2002.02-present	4900	50, 100, 150, 200, 250, 300, 350, 400, 450, 500, 600, 700, 800, 900, 1,000
RAMA-N	15	90	2007.11-2017.01	2700	1, 5, 10, 13, 16, 20, 40, 43, 50, 60, 80, 100, 120, 140, 180, 300, 500
RAMA-S	25	100	2012.08-2014.11	4800	1, 5, 10, 20, 40, 60, 80, 120, 140, 180, 300
IMOS	27	155	2015.05-present	4800	100, 150, 200, 300, 400, 450, 500, 800
Stratus	20	275	2000.10-2010.1	4400	5, 10, 15, 30, 40, 60, 85, 130, 190, 350, 450
PRIATA	19	325	2005.09-present	4200	1, 5, 10, 20, 40, 60, 80, 100, 120, 140, 180, 300, 500

Article

Extended Data Table 2 | Co-occurrence of subsurface MHWs with AEs and MCSs with CEs at the selected observation depths shown in Fig. 2

Site	Observation depth (m)	P _{CE} (P _{AE})	P _{MHWs_CE} (P _{MCSs_AE})	P' _{MHWs_CE} (P' _{MCSs_AE})	P _{SMHWs_CE} (P _{SMCSs_AE})	P' _{SMHWs_CE} (P' _{SMCSs_AE})
WHOTS	155	11% (17%)	61% (62%)	53% (48%)	76% (63%)	61% (56%)
KEO	475	9% (8%)	58% (35%)	44% (16%)	63% (29%)	58% (14%)
MOVE-3	200	16% (6%)	48% (45%)	41% (25%)	54% (44%)	60% (31%)
RAMA-N	300	12% (15%)	74% (67%)	45% (50%)	73% (75%)	57% (58%)
RAMA-S	300	15% (10%)	57% (40%)	48% (33%)	75% (67%)	57% (44%)
IMOS	800	12% (17%)	78% (73%)	41% (39%)	71% (86%)	54% (47%)
Stratus	450	15% (7%)	31% (33%)	23% (33%)	36% (25%)	26% (38%)
PRIATA	300	12% (12%)	69% (54%)	37% (43%)	67% (94%)	47% (43%)

The P_{AE} (P_{CE}) is the occurrence frequency of AEs (CEs). The P_{MHWs_AE} (P_{MCSs_CE}) is the ratio of MHW (MCS) events co-occurred with AEs (CEs). The P'_{MHWs_AE} (P'_{MCSs_CE}) is the percentage of MHW (MCS) days occurred within AEs (CEs). The P_{SMHWs_AE} (P_{SMCSs_CE}) and P'_{SMHWs_AE} (P'_{SMCSs_CE}) are the same as P_{MHWs_AE} (P_{MCSs_CE}) and P'_{MHWs_AE} (P'_{MCSs_CE}), respectively, but for more severe MHWs (MCSs) exceeding (falling below) 95th and 5th percentile temperature variability.